Applied and Environmental Microbiology, Dec. 2008, p. 7338–7347 Vol. 74, No. 23
0099-2240/08/$08.00+0 doi:10.1128/AEM.00631-08

Effect of Permeate Drag Force on the Development of a Biofouling Layer in a Pressure-Driven Membrane Separation System▽

L. Eshed,[1] S. Yaron,[2] and C. G. Dosoretz[1]*

Faculty of Civil & Environmental Engineering and Grand Water Research Institute[1] and Faculty of Biotechnology and Food Engineering,[2] Technion-Israel Institute of Technology, Haifa, Israel

Received 14 March 2008/Accepted 24 September 2008

The effect of permeate flux on the development of a biofouling layer on cross-flow separation membranes was studied by using a bench-scale system consisting of two replicate 100-molecular-weight-cutoff tubular ultrafiltration membrane modules, one that allowed flow of permeate and one that did not (control). The system was inoculated with *Pseudomonas putida* S-12 tagged with a red fluorescent protein and was operated using a laminar flow regimen under sterile conditions with a constant feed of diluted (1:75) Luria-Bertani medium. Biofilm development was studied by using field emission scanning electron microscopy and confocal scanning laser microscopy and was subsequently quantified by image analysis, as well as by determining live counts and by permeate flux monitoring. Biofilm development was highly enhanced in the presence of permeate flow, which resulted in the buildup of complex three-dimensional structures on the membrane. Bacterial transport toward the membrane by permeate drag was found to be a mechanism by which cross-flow filtration contributes to the buildup of a biofouling layer that was more dominant than transport of nutrients. Cellular viability was found to be not essential for transport and adhesion under cross-flow conditions, since the permeate drag overcame the effect of bacterial motility.

Membrane separation is becoming a wide-spread technology for water and wastewater treatment and purification (35). A membrane is basically a selective porous medium which allows the transfer of certain molecules to the permeate side based on size and charge depending on the type of process. In cross-flow membrane separation there are two simultaneous streams: the feed stream, flowing parallel to the membrane walls, and the permeate stream, flowing perpendicular to the membrane surface (Fig. 1).

The movement of particles, colloids, and nutrients toward the membrane surface enhances the development of a biofilm layer (biofouling). Besides the substances that have a biological origin, including cells and extracellular polymeric substances (EPS), the biofouling layer may include inorganic and organic substances and particulate material rejected by the membrane. Biofilms provide clear advantages to microorganisms, including protection from stress conditions in the environment, better metabolic cooperation, and higher densities that facilitate genetic exchange (15, 52). Biofouling can become a significant problem if biofilm growth is not controlled, because it can lead to clogging of a membrane, impairing the ability of the system to function properly (7).

In cross-flow membrane filtration, the net velocity of particles toward the membrane surface is determined largely by normal convection, and small contributions are made by tangential convection and Brownian diffusion (51). Nonspecific interfacial forces seem to dominate bulk transport and thus govern deposition phenomena. These interfacial forces are caused by interactions such as van der Waals, steric, Lewis acid-base, and electrostatic double-layer phenomena and hydrodynamic conditions (31). Compared to dead-end filtration, cross-flow filtration has the intrinsic advantage that the feed stream generates a tangential shear force on the membrane walls, thereby diminishing biofouling.

The initial attachment of bacteria on membranes is controlled largely by physicochemical factors, such as solution chemistry, surface properties of the membrane and particles, and the hydrodynamic conditions (2, 4, 9, 11, 18, 19, 34, 57). Bacterial factors also have an important role in attachment. Increased production of specific surface proteins and exopolysaccharides results in increased cellular adhesiveness and biofilm formation (28, 49, 53). The expression of these components is mediated by GGDEF domain-containing proteins in different bacteria, including *Pseudomonas putida*, *Escherichia coli*, *Salmonella enterica*, *Vibrio cholerae*, and *Pseudomonas aeruginosa* (23, 32). Surface attachment, especially in the early stages of colonization, may also be affected by bacterial motility, particularly twitching motility, a form of surface translocation mediated by flagella and type IV pili (14, 26, 42, 43). Flagella have been proposed to be important in the initial phase of attachment of *P. putida* to plant roots and fungal hyphae (55, 58), but they were not shown to be necessary on other surfaces (22). Moreover, a hyperflagellated mutant strain was shown to exhibit impaired initial biofilm formation (13). Flagella are also known to play a role in the structural development of a biofilm. Subsequent to the formation of microcolonies, flagellum-driven motility plays a key role in the formation of loose protruding structures (54). The expression of flagella was found to have a strong relationship to surface attachment; this expression is downregulated quickly after surface attachment and is upregulated at later stages of biofilm development (32).

Motility was found previously to be involved in bacterial

* Corresponding author. Mailing address: Faculty of Civil and Environmental Engineering, Technion-Israel Institute of Technology, Haifa 32000, Israel. Phone: 972 4 8294962. Fax: 972 4 8228898. E-mail: carlosd@tx.technion.ac.il.

▽ Published ahead of print on 17 October 2008.

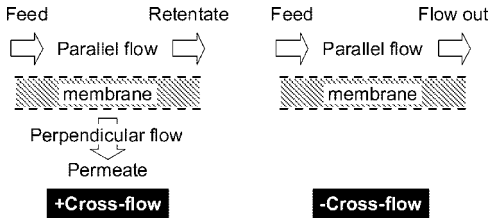

FIG. 1. Schematic diagram of cross-flow filtration (+Cross-flow) and non-cross-flow filtration (−Cross-flow). Under cross-flow filtration conditions there is a permeate stream which acts perpendicular to the feed stream, whereas under the non-cross-flow regimen there is unidirectional flow.

attachment to surfaces in both flowing systems (33, 39) and static systems (43, 47, 56). In a cross-flow regimen, there is a trade-off between the shear force (which acts in the horizontal direction and releases bacteria from the surface by shearing them off the surface) and the permeation drag force that originates from the pressure gradient across the membrane or transmembrane pressure (which acts in the vertical direction, carrying bacteria and other particles toward the membrane). So far, little is known about the importance of motility in bacterial attachment and biofilm development in cross-flow membrane filtration, which has a different flow field than the conventional flow pattern of unidirectional flow.

Not only is the permeation drag force, which acts perpendicular to the stream lines, an additional strong force assisting in penetration of the hydrodynamic layer by cells (18, 19), but it may also influence biofilm development, as follows: (i) by speeding up and enhancing attachment of the first cell clusters in the early attachment phase, (ii) by increasing the migration of nutrients and gases toward the base of the biofilm, and (iii) by improving the removal of metabolites and the spread of signal molecules. The influence of cross-flow on the physical properties or morphology of biofilms has not been thoroughly explored, yet both morphological and physical differences between biofilms grown with and without cross-flow can be expected due to the perpendicular flow vector. Biofilm thickness and density are two important parameters which may change in the presence of permeation due to an enhanced flux of nutrients. Changes in these parameters may result in diffusional limitations and affect the microenvironment surrounding the cells (46).

The working hypothesis of the present research was that the permeation drag force overcomes the local shear force and overshadows the importance of swarming motility in the adhering bacteria, making swarming motility irrelevant in this case. Once attached, the bacteria that colonize the membrane surface utilize the nutrient flux into biomass and form the EPS of the biofilm. Therefore, the aim of the present study was to investigate how cross-flow filtration quantitatively affects biofilm structural parameters in a bench-scale system consisting of tubular ultrafiltration membrane modules inoculated with fluorescently tagged *P. putida* S-12 and operated using a laminar flow regimen under sterile conditions in continuous mode. The biovolume, thickness, density, coverage area, and morphology, as well as the decrease in the permeate flux through the membrane during buildup of the biofouling layer, were determined. The effect of the cross-flow on microbial cell transport and the importance of motility during initial colonization were studied as well. These parameters were examined by using confocal scanning laser microscopy (CLSM) imaging and subsequent image analysis upon induction of biofilm formation.

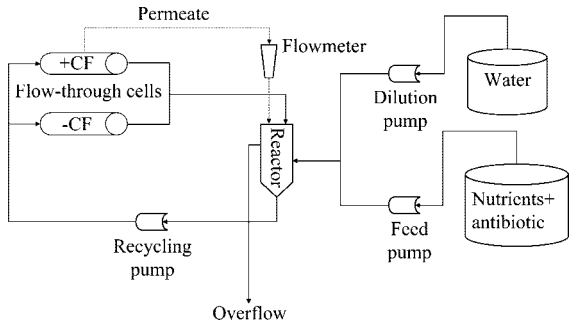

FIG. 2. Schematic diagram of the dual-channel tubular flowthrough cell system. Cells were 13 cm long and 12.5 mm in diameter. A concentrated nutrient fed solution was directly diluted with distilled water to obtain the desired concentration in a 140-ml reactor by regulating the flow of the feed and dilution peristaltic pumps. Pressure gauges and rotameters were used for continuous determination of membrane permeability. The system was run under sterile conditions. Membrane modules are in the upper left corner (Flow-through cells). Where indicated, a third membrane reactor was added.

MATERIALS AND METHODS

Bacterial strain. *P. putida* wild-type strain S-12 (= ATCC 700801) (27) was used as the model organism in this study. The minitransposon (plasposon) pTn*Mod*-RKm′ (GenBank accession number AF061930) was used as a suicide delivery vector to mark the *P. putida* S-12 chromosome with DsRed (red fluorescent protein [RFP]) and a kanamycin resistance gene (Kan^r) (17). A single-species biofilm was used in order to simplify the test system and provide a means for easier tracking of biofilm development without the influence of a relationship between different bacterial populations.

Inoculum and media. Luria-Bertani (LB) broth was used for the starter cultures (which were grown for 16 h at 30°C in shaken flasks) that were used for inoculation of the experimental cultures. The experimental medium consisted of LB broth diluted 1:75, unless otherwise indicated. The proper dilution was obtained by proportional addition of water and LB medium diluted 1:10 by using two peristaltic pumps. Kanamycin (30 μg/ml) was added to the maintenance, inoculum, and experimental media for selection.

The experiments were started by adding a volume of the starter culture (optical density, 3.3) to the reaction medium (140 ml) to obtain an initial cell concentration of approximately 1.4×10^7 cells/ml in the reactor (Fig. 2). All experiments were performed under sterile conditions.

Flowthrough cell system. A dual-channel tubular flowthrough cell system that allowed work under sterile conditions was used (Fig. 2). The flowthrough cells (length, 13 cm; diameter, 12.5 mm) were equipped with a tubular 100-kDa-molecular-mass-cutoff ultrafiltration membrane made of polyvinylidene difluoride (PF100; PCI). Unless indicated otherwise, one cell was run under cross-flow conditions (+CF), which allowed passage of permeate through the membrane, and the other was run without cross-flow (−CF) using unidirectional flow (Fig. 2). A concentrated nutrient feed solution was directly diluted with double-distilled water to obtain the desired concentration in a 140-ml reactor by regulating the flow of two parallel peristaltic pumps (Cole-Parmer, United States). The cells, reactor, and reservoirs were all made of Pyrex glass. The different components of the system were connected with silicone tubing, and recirculation was accomplished by using a peristaltic pump. The system was equipped with pressure gauges and rotameters.

Biofilms of *P. putida* were allowed to develop on the membrane surfaces as a model for biofouling layer development under sterile conditions. In all cases all the components of the system except the membranes and the pressure gauges were autoclaved (121°C for 20 min) prior to each experiment. After the system was assembled, a 0.5% (wt/wt) NaOCl solution was run in the system for at least 3 h, and then the system was thoroughly rinsed with sterile double-distilled water

for 16 h. In order to check for sterility, the rinse water was plated on LB agar plates prior to each experiment.

After inoculation the influent flow rate was maintained at 3.5 ml/min, resulting in a dilution rate of 0.025 h^{-1} (corresponding to a hydraulic residence time of 40 min). This rate was greater than the washout rate for *P. putida* S-12 in the diluted medium in order to minimize suspended growth and to encourage biofilm growth (48). Effluent samples were taken right after inoculation, and the concentrations were found to be approximately 10^7 cells/ml.

The average flow velocity ($\bar{u}$) was maintained at approximately 0.065 m/s, and the corresponding calculated Reynolds number was 910 (at 30°C) (i.e., laminar flow). The shear rate on the membrane surface (Γ_w) using the laminar flow regimen was calculated as follows: $\Gamma_w = 8\bar{u}/D = 41.6\ s^{-1}$, where D is the tubular membrane diameter.

Permeability (L_p) is defined as the specific permeate flux (J) through a membrane relative to the transmembrane pressure drop (ΔP) across the membrane and was calculated as follows: $L_p = J/\Delta P$ (liters/m^2 · h-10^5 Pa) (neglecting osmotic pressure changes). Permeability was calculated at different time points in order to track the kinetic pattern of the biofouling layer buildup showing blockage of the membrane. The transmembrane pressure was calculated as follows: $\Delta P = (P_{in} + P_{out})/2$ (neglecting the pressure on side of the permeate, which was discharged at atmospheric pressure), where P_{in} and P_{out} are the pressure of the feed stream and the pressure of the retentate stream, respectively (Fig. 2). Unless indicated otherwise, the experiments were conducted at a fixed initial ΔP of 10^5 Pa.

A sampling port was located in the overflow line at the exit of the reactor.

Autoclave-sterilized 0.22-μm air filters (Millipore Millex-FG50) were located on the reactor and the feeding carboys to allow free aeration of the system.

Comparative growth of biofilms on membranes with and without cross-flow. Independent experiments were performed for different time periods (1 h up to 6 days), and in each experiment side-by-side +CF and −CF membrane modules were used. The system was prerun with a nutrient solution for 4 h in filtration mode (i.e., with permeate flux) prior to inoculation (time zero). After inoculation as described above, a sample of the liquid in the system was collected and plated to determine the live cell count. The permeate flow rate for the +CF membrane was recorded during the experiments at different time points, as indicated below.

At the end of each experiment, the membranes were removed from the system and were thoroughly washed with a sterile saline solution to remove all loosely attached bacteria. To count the attached bacteria, two 1-cm-long pieces (area of each piece, 3.93 cm^2) from each membrane were vortexed in a glass tube for 40 s with 4.5 ml of saline containing 0.1% Tween 80 and 2.5 g of glass beads (diameter, 3 mm). Serial dilutions were prepared and plated on LB agar plates. The plates were incubated at 30°C for 16 h. To analyze the biofilm structure, membrane samples were sliced and prepared for microscope analyses as described below.

Effect of the permeate drag force on bacterial transport and biofilm formation. To determine the effect of the permeate drag force on bacterial transport and biofilm formation, a flowthrough system that was similar to that described above but included three parallel channels was used. The system was prerun with a nutrient solution for 4 h and aseptically inoculated (time zero), as described above. After inoculation, a sample of the liquid in the system was collected and plated. Then all three modules were operated as +CF membrane modules for 15 min, allowing a flux of permeate through the membrane, in order to allow bacteria to attach equivalently to all three membranes in full recycle mode (batch mode). During this phase no fresh nutrients were introduced into the system in order to keep the bacterial concentration in the system constant. After this the system was aseptically evacuated and then refilled with fresh nutrients (purging phase). This procedure was repeated at least five times for 1 h in order to remove the maximum number of planktonic cells possible. At the end of this phase, a sample of fluid was collected from the system and plated in order to determine the concentration of suspended bacteria left in the system. Concomitantly, one module was removed from the system, and the membrane in it was thoroughly washed with a sterile saline solution to remove loosely attached bacteria, as described above, and plated to quantify the attached bacteria. From this point onward, the nutrient feed rate was increased to 1.5 liters/h (retention time, 8 min) in order to wash out all remaining planktonic bacteria.

One of the two modules left was run as a +CF module and the other was run as a −CF module, as described above, for an additional 4 h. At the end of this period a sample of each liquid was collected and plated in order to determine the suspended cell concentration in the system, which was found to be approximately 10^4 cells/ml, which was 3 orders of magnitude less than the concentration right after inoculation. Then the two modules were removed, and the membranes were washed and plated as described above.

Influence of bacterial viability on adherence to the membranes. Two separate flowthrough cell systems were run in parallel under sterile conditions. One of these flowthrough systems was a dual-module system similar to that shown in Fig. 2, and it was inoculated with dead cells (as described below); one module contained a +CF membrane, and the other module contained a −CF membrane. The second flowthrough system was a single-module system that was inoculated with only live cells (+CF). Both systems were inoculated so that the final cell concentrations were the same. In this setup, both systems were operated by using a three-head peristaltic pump (Cole-Parmer) under flow conditions that were the same as those described above. The running time was 1 h in order to allow early attachment while minimizing duplication of the live bacteria. After inoculation, a sample of the liquid in the system was collected and plated. Both systems were run with full recycling (batch mode) in order to avoid differential dilution and washout.

At the end of the running time the membranes were removed and thoroughly washed with a sterile saline solution. Membrane specimens were cut, thoroughly washed, and directly observed with a fluorescent microscope to analyze the coverage area.

For preparation of live and dead RFP-tagged *P. putida* S-12 cell suspensions, bacteria were grown and harvested as described by Solomon and Matthews (50). Briefly, cells were grown overnight in LB medium and then split into two parts. Cells were killed with 2.5% glutaraldehyde, and microscopic observation showed that the dead cells retained their fluorescence properties.

Microscopy. (i) CLSM. Biofilm development was visualized by using an MRC 1024 CLSM (Bio-Rad, Hempstead, United Kingdom) equipped with a Nikon Plan Apo 63x1.40 objective and by using a Zeiss 510 Meta confocal laser scanning microscope equipped with a Zeiss AxioImager Z1 equipped with detectors, lenses, and filter sets for monitoring fluorescent staining. The EPS was visualized by using concanavalin A (fluorescein isothiocyanate) staining (40, 41). Bacterial cells were visualized by using RFP tagging. Staining with the nucleic acid stains Syto9 (S34854; Invitrogen-Molecular Probes) and propidium iodide (P4170; Sigma) for visualization of total cells and dead cells, respectively, was performed according to the manufacturers' instructions.

The parameters for the CLSM were set once and applied evenly as much as possible for the rest of the experiments in order to ensure that there could be quantitative comparison of the results. Wavelengths were set by using the manufacturers' instructions, as follows: for concanavalin A (fluorescein isothiocyanate) and Syto9, excitation at 488 nm and emission at 498; for RFP, excitation at 563 and emission at 580 nm; and for propidium iodide, excitation at 493 and emission at 630.

(ii) Fluorescent microscopy. Early stages of biofilm development were tracked by observation of fluorescently tagged bacteria using a Leica Dmire2 inverted microscope and a Zeiss Axio-observer 200 M inverted microscope. *z* cross sections were acquired by using ×40 and ×63 lenses (*z* cross sectioning was needed due to the curved nature of the membrane surface).

(iii) SEM. Membrane samples used for scanning electron microscopy (SEM) were fixed with glutaraldehyde and dehydrated using an ethanol gradient under cold conditions, as described elsewhere (3, 30). To dry the cells, hexamethyldisilazane was used instead of critical point drying. This method has been reported to be more suitable for drying samples of cells for SEM examination without causing disruption of the cell structure (3). Samples were sputter coated with carbon and were visualized by using a Leo Gemini 982 high-resolution SEM. All chemicals employed were electron microscopy quality (Sigma Chemical, St. Louis, MO).

(iv) Image analysis. PHLIP software (38; http://phlip.sourceforge.net) is an open-source software which was specifically designed for three-dimensional (3D) biofilm analysis. PHLIP automatically sets the threshold value using the Otsu algorithm (44) and calculates the architectural parameters. PHLIP runs on the Matlab platform and requires an additional definitions file, which was automatically produced by Auto-PHLIP-ML software (37; http://sourceforge.net/projects/auto-phlip-ml). Auto-PHLIP-ML also removes bias from biologically insignificant pixels by removing extraneous images.

In this work PHLIP calculations were used to determine the biovolume, substratum coverage, area-to-volume ratio, and mean thickness. Biovolume is the volume of the biomass, as measured by accumulation of foreground pixels which are attributed to biomass (by external fluorescent staining or inherent bacterial RFP). The threshold was set automatically by PHLIP (by running the Otsu algorithm) and was manually verified and adjusted when necessary (38).

PHLIP was run in the "no connected volume filtration" (CVF) mode. The CVF option removes pixels that are not connected to the substratum through connection to other neighboring pixels (38). In our study CVF was found to cause bias in the results due to the curved membrane surface. Data were exported in an XML format and were statistically analyzed using Excel.

ImageJ (http://rsb.info.nih.gov/ij/) was used for 3D imaging (using the "Volume Viewer 1.31" plugin [6; http://rsb.info.nih.gov/ij/plugins/volume-viewer

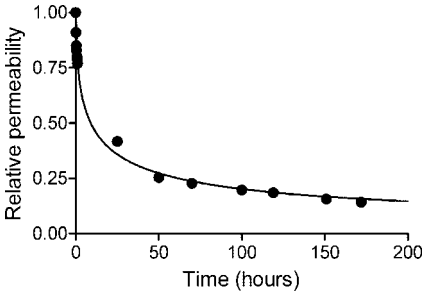

FIG. 3. Typical time profile for the relative permeability of a +CF membrane due to the buildup of the biofouling layer. The asymptotic value of the permeate flux corresponds to the fully developed biofilm (biofouling) layer. The initial permeability was 0.6 ± 0.06 liter/m^2 · h-10^5 Pa.

.html]) and for analysis of the coverage area at the early development stages (monolayer) of the biofilm.

z stack images acquired by fluorescent microscopy were processed and focused by using the "Extended depth of field" plugin (21; http://bigwww.epfl.ch/demo/edf/#soft) to produce a focused merged image of the whole scanned area for subsequent coverage area analysis.

RESULTS

Effect of cross-flow on the buildup, morphology, and structural parameters of biofilms that developed on membranes. The purpose of these experiments was to perform a comparative study of biofilm development on membranes with and without cross-flow filtration. The −CF membranes did not have a pressure gradient across them, which prevented permeate flux as well as the accumulation of a concentration-polarization layer. In the +CF membranes there was a pressure difference across the membranes, and consequently permeate flux was allowed, generating a convective flow toward the membrane surface.

The bacterial adherence and buildup of the biofilm layer on the +CF membranes resulted in a typical exponential decrease in the membrane permeability, and there was a ~75% decrease after 48 h (Fig. 3). Following this, the permeability reached an asymptotic value, which corresponded to the value for a fully developed biofilm (i.e., saturation resistance was reached under these conditions). We predicted that a decrease in permeability would occur shortly after inoculation. Measurement of the permeate flux in several independent replicate experiments showed that a 22% decrease in permeability occurred within the first hour once bacterial deposition and biofilm formation occurred, and after this the decrease was moderate (Fig. 3).

The biofilm buildup was more evident on the +CF membranes, as shown by the greater thickness of the biofilms grown on the +CF membranes than of the biofilms grown on the −CF membranes (Table 1). Within 12 h after inoculation, the biofilm on a +CF membrane consisted of a thin layer of cells (varying from a monolayer up to 8 μm thick), while the biofilm on a −CF membrane consisted of a sparse layer of cells which randomly colonized the membrane surface. The difference between the biofilms on the +CF and −CF membranes was also observed at 20 h, although both biofilms were denser. At ≥6 days, the +CF membranes became clogged by the biofilm layer, the permeate flux decreased to negligible levels (Fig. 3), and the hydraulic conditions in the membranes approached those in −CF membranes (in terms of cross-flow performance). During this time, the cells attached to the −CF membranes developed a complex 3D structure, and the thickness of the biofilms increased; however, the biofilms were not as thick as the biofilms on the +CF membranes. The variability in the thickness of the biofilms on the −CF membranes after 6 days was significantly greater than the variability in the thickness of the biofilms on the +CF membranes, as shown by the standard deviations (Table 1). This finding correlated with the higher frequency of bare patches on the −CF membranes compared to the greater homogeneity of the coverage on the +CF membranes.

The morphology of the mature biofilms, as determined by CLSM and high-resolution SEM, included a complex and filamentous 3D structure, including cavelike structures and tunnels, which presumably allowed the transfer of nutrients and gases toward the base of the biofilms (Fig. 4). This structure is common in biofilms developing in fast-flow environments, as reported previously (52).

The bacterial densities of the biofilms that accumulated on the membranes were determined by obtaining plate cells counts, normalized to either the membrane surface area (Fig. 5) or the biovolume (Table 1). The bacterial density (based on the surface area covered) for both +CF and −CF membranes increased as the biofilm developed, as expected. However, a difference of more than 5 orders of magnitude between −CF and +CF membranes was seen at the early attachment stage at 1 h postinoculation (Fig. 5). The difference gradually decreased with time; after 12 h the +CF membrane biofilms were 3 orders of magnitude denser than the −CF membrane biofilms, and after 6 days the +CF membrane biofilms were 1.5 orders of magnitude denser than the −CF membrane biofilms. The decrease in the difference correlated with the convergence over time of the two systems toward a −CF membrane-like regimen and indicates that there

TABLE 1. Biofilm properties

Time (h)	Thickness (μm)[a]			Bacterial density (CFU/μm^3)[b]		Bacterial biovolume/EPS biovolume ratio[c]		
	+CF	−CF	*t* test	+CF	−CF	+CF	−CF	*t* test
12	8.5 ± 4.9	2.9 ± 1.8	0.0164	2.0×10^{-2}	1.2×10^{-5}	0.8 ± 0.6	ND[d]	
20	13.5 ± 4.4	5.5 ± 3.5	0.0021	2.5×10^{-2}	2.8×10^{-3}	0.9 ± 0.3	1.2 ± 0.5	0.2296
144	40.5 ± 1.2	20.4 ± 15.1	0.1475	3.7×10^{-1}	1.0×10^{-1}	8.6 ± 4.9	4.0 ± 2.2	0.0583

[a] Biofilm thickness was determined by CLSM. The values are the means ± standard deviations of 15 replicates.
[b] Bacterial density was expressed as the number of CFU normalized to the biovolume for at least two independent experiments in which at least 10 measurements were obtained for each type of membrane. Standard deviations could not be computed and a *t* test could not be performed since bacterial cell counting was done independent of biovolume measurement.
[c] The values are the ratios of the bacterial biovolume to the EPS biovolume.
[d] ND, not detectable.

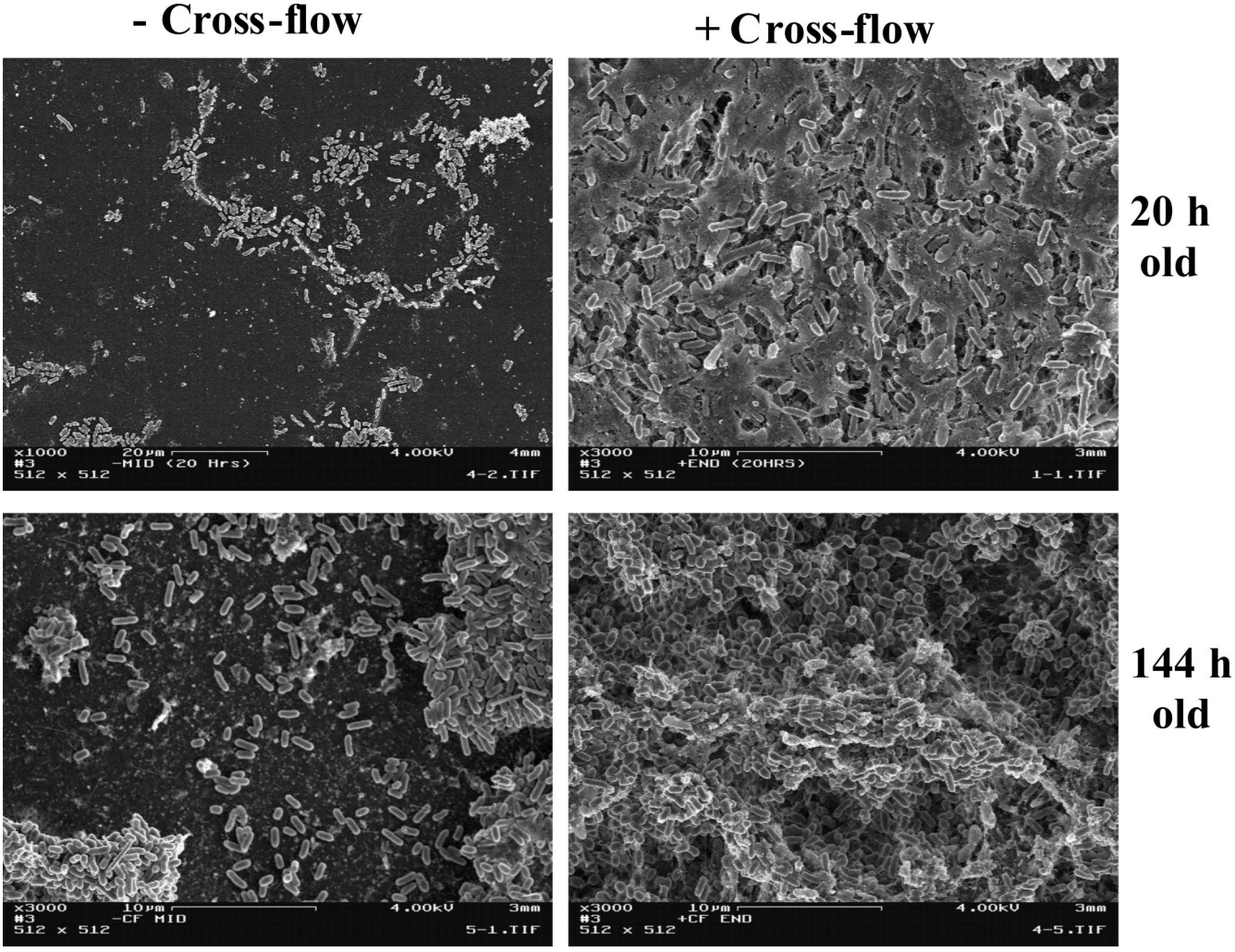

FIG. 4. Field emission SEM micrographs of 20- and 144-h-old biofilms grown under cross-flow and non-cross-flow conditions. After 20 h, there were noticeable differences in the coverage area and biofilm development. After 144 h, both biofilms had developed a complex 3D structure. However, on the −CF membrane there were still areas that were not fully covered.

was a saturation level for colonizing bacteria and reproduction and detachment of the anchored bacteria under the hydrodynamic conditions used. As stated above, the higher concentration of cells on the +CF membranes was explained by the convection force of the permeate stream, which actively transported bacteria toward the membrane surface.

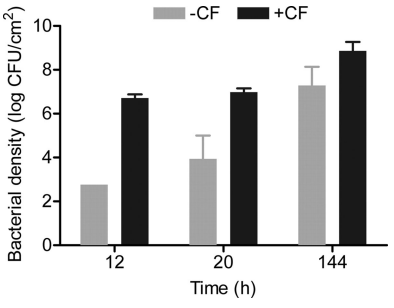

FIG. 5. Bacterial densities of biofilms at different times, expressed as live counts per area of the membrane. The values are the averages for at least four independent measurements obtained in four independent experiments performed as a set of two parallel runs each time. The error bars indicate standard deviations. The bacterial densities for the −CF membrane at 12 h are estimates, since the values were below the detection limit.

The increase in biofilm density was also apparent when the increase in bacterial density normalized to biovolume was examined. The biovolume increased less than the cell count, and it was apparently limited to a saturation value for the hydrodynamic conditions used (namely, the shear rate). As a consequence, the biofilm became denser as it developed.

In addition, a gradual change in the biofilm composition that took place during development may have contributed to the change in the increase in the bacterial density observed. Indeed, this was shown by the data for the biovolume of the bacterial biomass relative to the data for the biovolume of the EPS in a biofilm, which changed with time as the biofilm became denser (Table 1). For a +CF membrane, at the early stages (12 and 20 h) the same amounts of EPS and bacteria were found (ratio, 1:1). After 6 days the ratio increased in favor of the bacterial biomass, as the biofilm became denser.

On a −CF membrane, after 12 h a layer with a low bacterial density instead of a defined biofilm had formed, and this was taken into account when the biovolume ratio was calculated.

After 20 h the bacterial density had increased, and the ratio was close to the ratio obtained for the +CF membrane. After 6 days the −CF membrane biofilm had a developed structure, in which most of the biovolume was bacterial biovolume. The ratio of bacterial biovolume to EPS biovolume for the +CF membrane biofilm, which was denser than the −CF membrane biofilm, was twofold higher than the ratio for the −CF membrane biofilm.

The relative locations and amounts of the different components of biofilms (such as EPS, protein, and bacteria) are also of interest, since they determine the physical stability and tolerance of biofilms to different stress conditions. Differential CLSM observations and subsequent image analysis showed that a mature biofilm (i.e., a biofilm that was 6 days old) was surrounded by EPS that was 2 to 3 μm thick, whereas the bottom portions were composed mostly of bacterial biomass (Fig. 6). The EPS layer has been reported to be a protective layer (20, 52). At an early stage of development (when the biofilm was 20 h old), about one-half of the biovolume was EPS biovolume, mostly located toward the external surface of the biofilm (Fig. 7), while the internal portions were composed mostly of bacterial biovolume. This phenomenon was characteristic of biofilms on both the +CF and −CF membranes, depending on the rate of development.

Importance of the permeate drag force as a means of bacterial transport and nutrient flux toward the membrane surface. The permeate drag force augments the transfer of bacteria toward the membrane surface, as well as the flow of nutrients and adsorbed gasses through the membrane surface, providing the attached bacteria with a constant supply of nutrients and oxygen. These two processes occur simultaneously when cross-flow filtration is present. The purpose of this part of the study was to evaluate the contribution of each of these two processes to the buildup of the biofilm layer.

In order to evaluate the cross-flow permeate drag force as a means of bacterial transport, the system was inoculated and operated for 1 h with and without cross-flow. This time was long enough to allow the bacteria to attach to the membranes but short enough to avoid significant reproduction of the adherent bacteria. Plate count data showed that there was a 5-order-of-magnitude difference between the two types of membranes (1.3×10^6 cells/cm^2 attached to the +CF membranes and <12 cells/cm^2 attached to the −CF membranes). This difference in the density of adherent cells was also shown by microscopic observations (Fig. 8).

In order to evaluate the importance of the cross-flow permeate force in supplying a flux of nutrients and dissolved gases, an experiment was performed in which three replicate membranes were operated as +CF membranes for the first 15 min after inoculation, which allowed identical passage of the permeate. Then the system was thoroughly washed to remove planktonic bacteria, and one membrane was removed for plate counting (control for initial colonization). The two remaining membranes were then operated as +CF and −CF membranes for additional 4 h. This setup allowed similar initial bacterial colonization of the membranes, during which the permeate stream supplied nutrients and gasses. The plate count for the +CF membrane was $13.0 \times 10^6 \pm 1.1 \times 10^6$ cells/cm^2, which was 5-fold higher than the plate count for the −CF membrane ($2.30 \times 10^6 \pm 0.09 \times 10^6$ cells/cm^2) and 12-fold higher than the

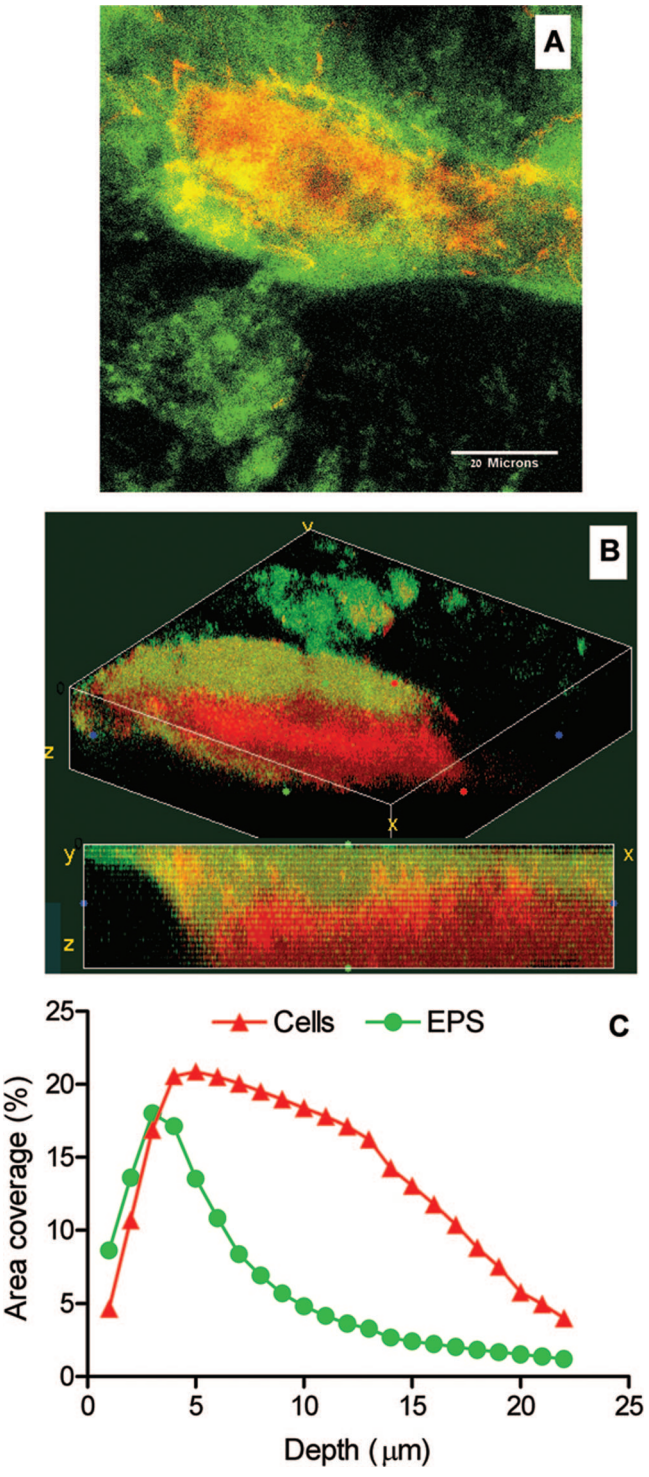

FIG. 6. Biofilm structure. (A) Typical CLSM micrograph of a 144-h-old −CF biofilm (maximal-intensity merged image of the *z* stack). The EPS cover the bacteria. (B) 3D image of the biofilm structure. (C) Relative levels of the EPS and bacteria as measured by coverage area at different *z* depths. The total thickness was 22 μm (1 μm per cross section). Note that for the first three cross sections the EPS are more abundant, while for all the other cross sections the bacterial biovolume is dominant.

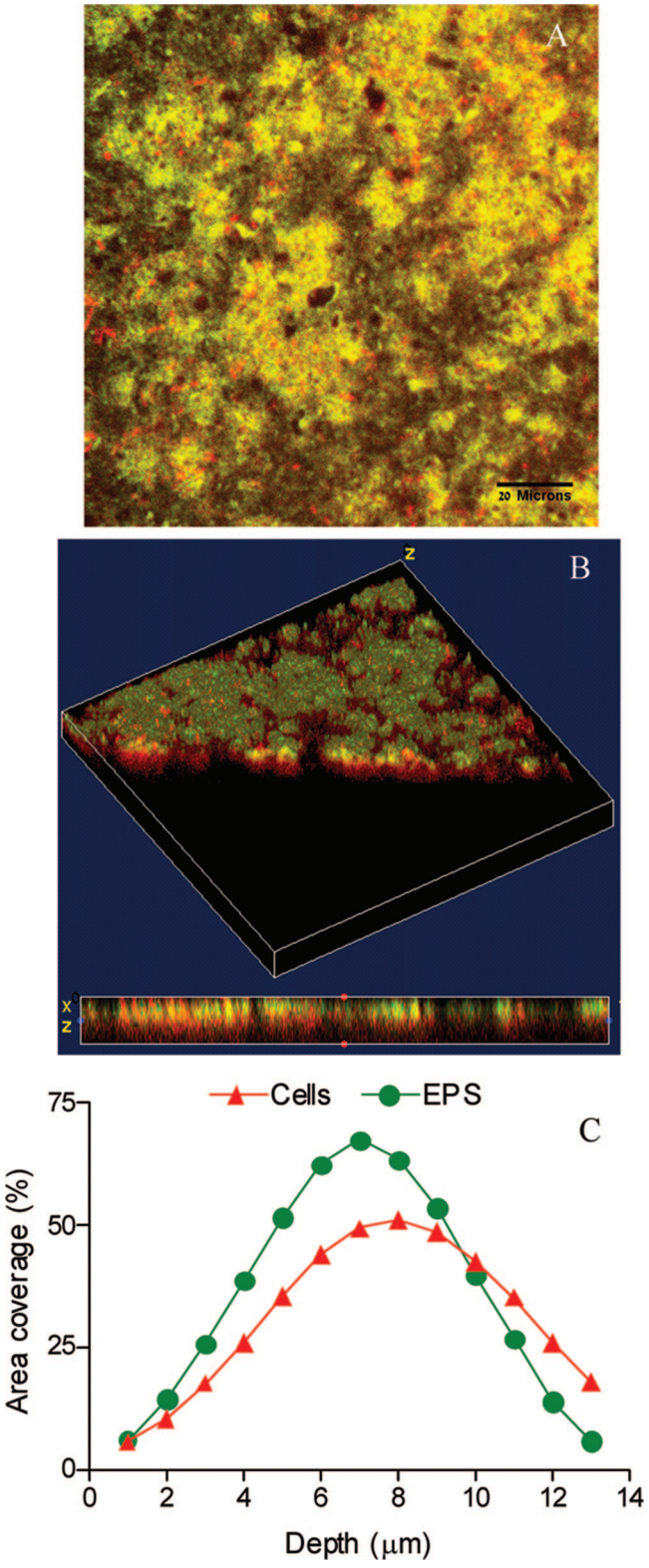

FIG. 7. Typical image of a 20-h-old +CF biofilm. (A) Maximal-intensity merged image of the *z* stack. (B) 3D image of the biofilm structure, cut in the middle of the biofilm. (C) Relative levels of the EPS and bacteria as measured by coverage area at different *z* depths. The total thickness was 13 μm (1 μm per cross section). Note that for the first nine cross sections the EPS was more abundant, while for the other cross sections bacterial biovolume was predominant.

plate count for the control membrane ($1.10 \times 10^6 \pm 0.01 \times 10^6$ cells/cm^2). As shown by a comparison of the −CF and control membranes, net cell growth equivalent to one doubling (i.e., potential biofilm growth) took place at the membrane surface. However, as shown by a comparison of the +CF and control membranes, the replication of the bacteria was approximately 12-fold greater on the +CF membrane. Hence, the contribution of permeation to the supply of nutrients to the bacteria colonizing a membrane resulted in a 0.5-order-of-magnitude increase for a 4-h time period, resulting in a ratio of more than 1:6 in favor of permeation as a means of bacterial transport toward the membrane surface.

In conclusion, these results clearly indicate that the cross-flow convective force enhanced bacterial transport (resulting in a 5-order-of-magnitude increase in bacterial density on the membrane within 1 h), while the increase in bacterial density due to transport of nutrients to the biofilm was only 0.5 order of magnitude after 4 h.

Adherence of live bacteria to the membrane surface under cross-flow conditions. This part of the study was aimed at evaluating quantitatively the contribution of the early attachment of living bacteria to the membrane surface under cross-flow conditions. To do this, the adhesion of live bacteria after 1 h and the adhesion of dead bacteria after 1 h were compared. Surface coverage analysis showed that +CF membranes were covered to almost the same extent, regardless of cell viability (for live bacteria, 14.0% ± 5.9% of the area was covered with bacteria; for dead bacteria, 19.6% ± 12.7% of the area was covered with bacteria), while −CF membranes were covered to a much lesser extent (0.5% ± 0.7% for dead cells and similar results for live cells, as determined in other experiments). Dead cells even appeared to cover more area than live bacteria in two different experiments (Fig. 9), but the difference was not statistically significant. This difference can be explained by changes in the net charge and surface properties of the glutaraldehyde-inactivated cells upon interaction with the membrane surface compared with the net charge and surface properties of live bacteria (10, 29). In the case of −CF membranes very low levels of cell adherence, as shown by the low coverage area, were obtained with dead cells (Fig. 9C) and live cells (Fig. 8). Overall, these findings clearly indicate that the convective force driven by the cross-flow is the dominant factor responsible for transport of bacterial cells (and other similar colloids) to the membrane.

DISCUSSION

Cross-flow is an important process in water and wastewater membrane separation systems in which the main stream (feed) flows parallel to the membrane walls, while the permeate stream flows perpendicular to the feed stream, toward the membrane wall. A major operational problem in this process is the buildup of a biofouling layer, which blocks the membrane and causes significant losses of energy. In order to study the contribution of the permeation drag force to the creation of a biofouling layer, a tubular flowthrough cell system, mimicking simple pipe flow conditions, with and without permeate flow was used. We found that membranes operating with a cross-flow regimen were colonized very rapidly and that there was an approximately 22% reduction in the permeate flux within the

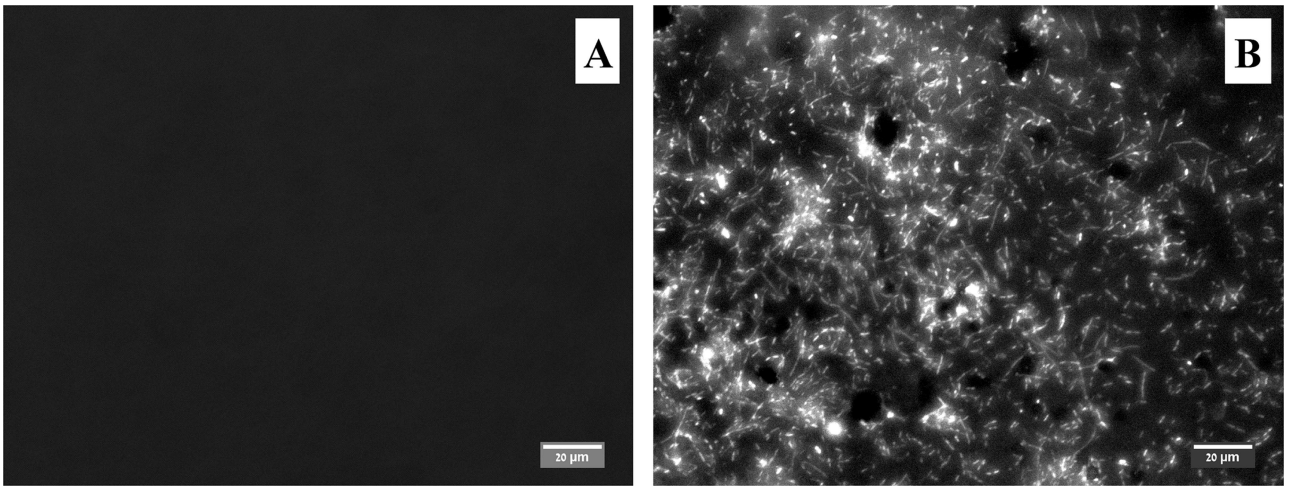

FIG. 8. SEM micrographs of a −CF membrane (A) and a +CF membrane (B) after 1 h of running time. Bacteria are adhering to the surface of the +CF membrane, while the −CF membrane has no adherent bacteria.

first hour. These findings are in line with previous observations for membrane colonization, which occurred within minutes (34). In the absence of permeation (i.e., with only parallel flow), the deposition of bacteria was slower since the planktonic bacteria had to overcome the parallel drag forces to reach the surface, as in the generic case of biofilm initiation in flowing systems, and consequently the biofilm developed slowly. Similarly, Kang et al. (31) reported that even in the absence of a permeate stream there was deposition of bacteria on a membrane.

Structural parameters of the biofilm layer, such as thickness, biovolume, and bacterial density, increased gradually as the biofilm developed. Interestingly, the differences in these parameters between the +CF and −CF membranes gradually decreased with running time, and the values converged to similar levels after 6 days of operation. This convergent time profile can be explained by two processes that occurred in parallel: (i) as planktonic cells attached to the membrane, settled, and started to form a biofilm (~12 to 20 h), the +CF membrane became clogged and the permeate flux decreased exponentially, resulting in a lower permeate drag force that transported bacteria and dissolved nutrients to the membrane surface; and (ii) the biofilm on the −CF membrane developed slowly in a conventional biofilm pattern under diffusive conditions. Moreover, the hydraulic conditions used (retention time less than the doubling time of planktonic cells) favored proliferation of attached bacteria versus planktonic bacteria, whose concentration in the system consequently decreased. These events gradually reduced the influence of convection forces toward the membrane surface due to permeate flux.

Our findings further show that transport of bacteria to the membrane surface (by a convection force) is the main cause of biofilm enhancement, while the flux of nutrients to the biofilm is a less important mechanism. This effect is most significant in the early stages of the biofilm development, when the active transport of planktonic cells toward the membrane surface is maximal and the dependence of the attached bacteria (still in a monolayer) on a nutrient flux is less crucial. Once the biofilm has fully developed, the dominant contribution of the permeate stream is nutrient supply, even though at this stage the permeate flux is significantly lower than that at the early stages. Therefore, both effects of permeation are important to biofilm development, but their relative magnitudes differ in the different phases of development.

Twitching and swarming motility have been found to be important for cell aggregation (25, 43) and hence for the development of biofouling, especially in the early stages (12, 55). Therefore, dead cells are not thought to be able to actively adhere but are dependent on adsorption due to chemical interaction forces (31) and the presence (or absence) of a permeation drag force. *P. putida* exhibits surface motility similar to swarming at room temperature (18 to 28°C), the temperature used in this research. At this temperature (but not at 30°C) the bacteria produce type IV pili and a polar flagellum. *P. putida* exhibits flagellum-independent surface movement, but the pili and lipopolysaccharide-O antigen are required for surface movement (36). Although these results were obtained for *P. putida* KT2440, the only fully sequenced *P. putida* strain, they may be applied to *P. putida* S-12. Indeed, microarray hybridizations showed that S-12 exhibits the highest level of genomic similarity to KT2440 (5). Our results indicate that in the case of cross-flow filtration, the permeation drag force overcomes the need for bacterial motility, and therefore, equal amounts of dead cells and live cells reach the membrane surface. This suggests that under the influence of the permeation drag force, self-motility is not essential for primary colonization.

A study of four strains of bacteria that produce biofilms on reverse-osmosis membranes suggested that in the presence of permeation, convective permeate flow reduces the dependence of bacterial cells on flagellum-mediated swimming motility in establishing the initial cell-to-surface contact (45). Our findings support this hypothesis. In a static system, flagellar motility is important for *P. aeruginosa* surface attachment, whereas type IV pili facilitate microcolony formation (43). However, type IV pili and flagellar motility do not significantly affect biofilm formation in a system with a constant flow (16). This suggests that cells subjected to shear force have limited surface move-

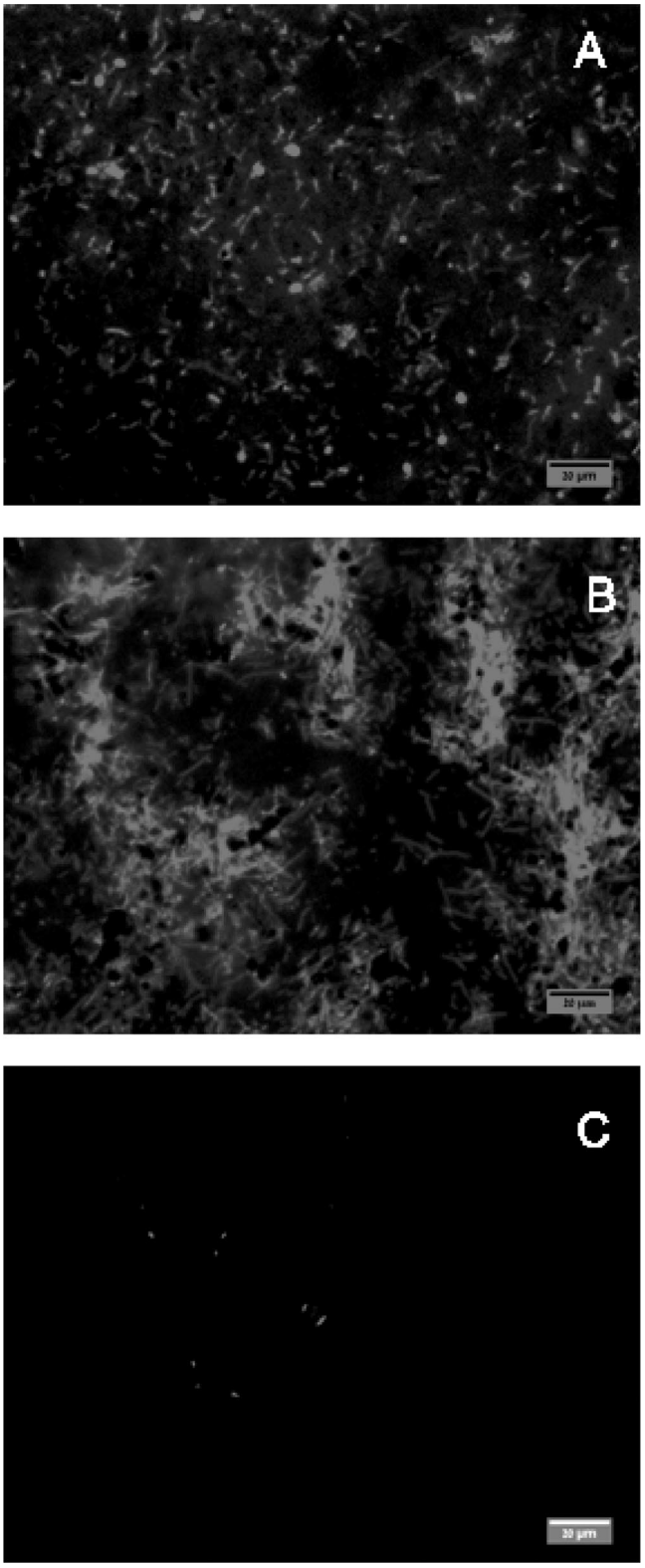

FIG. 9. CLSM micrographs of live (A) and dead (B) cells deposited under cross-flow filtration conditions and of dead cells under non-cross-flow filtration conditions (C). Note the lower number of bacteria attached without cross-flow. Analysis of live cells grown under non-cross-flow filtration conditions resulted in a similar image.

ment via type IV twitching motility and that the initial microcolony formation is affected mostly by other mechanisms, primarily cellular division, rather than by a combination of cell clustering and division.

In conclusion, our findings indicate that in membrane separation systems containing considerable loads of microorganisms (such as seawater desalination plants and wastewater treatment plants, in which the bacterial concentrations are 10^5 to 10^6 CFU/ml), the convective transport of bacteria to the membrane remains the main cause of biofilm formation. Furthermore, our results suggest that bacteriostatic pretreatment of the feedwater to reduce bacterial colonization may not be very helpful in membrane facilities, since the dead cells are deposited on the membrane wall and cause clogging. Thus, efficient removal of feed microorganisms by physicochemical and/or physical separation should be performed. Yet limiting nutrient availability in the feed seems to be the most effective countermeasure for biofouling control as nutrients represent potential biomass.

ACKNOWLEDGMENTS

This work was supported by the Fund for Promotion of Research at the Technion and Grand Water Research Institute, Technion, Haifa, Israel, and by the Infrastructure Program of the Ministry of Science and Technology of Israel.

We are grateful to Shiri Klein for providing the bacteria used in this study.

REFERENCES

1. Reference deleted.
2. **Al-Ahmad, M., F. A. A. Aleem, A. Mutiri, and A. Ubaisy.** 2000. Biofuoling in RO membrane systems. Part 1. Fundamentals and control. Desalination **132:**173–179.
3. **Araujo, J. C., F. C. Teran, R. A. Oliveira, E. A. Nour, M. A. Montenegro, J. R. Campos, and R. F. Vazoller.** 2003. Comparison of hexamethyldisilazane and critical point drying treatments for SEM analysis of anaerobic biofilms and granular sludge. J. Electron Microsc. **52:**429–433.
4. **Baker, J. S., and L. Y. Dudley.** 1998. Biofouling in membrane systems—a review. Desalination **118:**81–89.
5. **Ballerstedt, H., R. J. M. Volkers, A. E. Mars, J. E. Hallsworth, V. A. Martins dos Santos, J. Puchalka, J. van Duuren, G. Eggink, K. N. Timmis, J. A. M. de Bont, and J. Wery.** 2007. Genomotyping of *Pseudomonas putida* strains using *P. putida* KT2440-based high-density DNA microarrays: implications for transcriptomics studies. Appl. Microbiol. Biotechnol. **75:**1133–1142.
6. **Barthel, K. U.** 2007. Volume Viewer plugin for ImageJ, V1.31. FHTW, Berlin, Germany.
7. **Bishop, P. L.** 2007. The role of biofilms in water reclamation and reuse. Water Sci. Technol. **55:**19–26.
8. Reference deleted.
9. **Bos, R., H. C. van der Mei, and H. J. Busscher.** 1999. Physico-chemistry of initial microbial adhesive interactions—its mechanisms and methods for study. FEMS Microbiol. Rev. **23:**179–230.
10. **Bowen, W. R., A. S. Fenton, R. W. Lovitt, and C. J. Wright.** 2002. The measurement of *Bacillus mycoides* spore adhesion using atomic force microscopy, simple counting methods, and a spinning disk technique. Biotechnol. Bioeng. **79:**170–179.
11. **Characklis, W. G., and K. C. Marshall.** 1990. Biofilms. Wiley, New York, NY.
12. **Chen, G., and K. A. Strevett.** 2003. Microbial surface thermodynamics and interactions in aqueous media. J. Colloid Interface Sci. **261:**283–290.
13. **Choy, W. K., L. Zhou, C. K. Syn, L. H. Zhang, and S. Swarup.** 2004. MorA defines a new class of regulators affecting flagellar development and biofilm formation in diverse *Pseudomonas* species. J. Bacteriol. **186:**7221–7228.
14. **Costerton, J. W., P. S. Stewart, and E. P. Greenberg.** 1999. Bacterial biofilms: a common cause of persistent infections. Science **284:**1318–1322.
15. **Davey, M. E., and A. G. O'Toole.** 2000. Microbial biofilms: from ecology to molecular genetics. Microbiol. Mol. Biol. Rev. **64:**847–867.
16. **De Kievit, T. R., R. Gillis, S. Marx, C. Brown, and B. H. Iglewski.** 2001. Quorum-sensing genes in *Pseudomonas aeruginosa* biofilms: their role and expression patterns. Appl. Environ. Microbiol. **67:**1865–1873.
17. **Dennis, J. J., and G. J. Zylstra.** 1998. Plasposons: modular self-cloning minitransposon derivatives for rapid genetic analysis of gram-negative bacterial genomes. Appl. Environ. Microbiol. **64:**2710–2715.

18. **Flemming, H. C.** 2002. Biofouling in water systems—cases, causes and countermeasures. Appl. Microbiol. Biotechnol. **59:**629–640.
19. **Flemming, H. C., G. Schaule, T. Griebe, J. Schmitt, and A. Tamachkiarowa.** 1997. Biofouling—the Achilles heel of membrane processes. Desalination **113:**215–225.
20. **Flemming, H. C., and J. Wingender.** 2001. Relevance of microbial extracellular polymeric substances (EPSs). Part I. Structural and ecological aspects. Water Sci. Technol. **43:**1–8.
21. **Forster, B., D. Van de Ville, J. Berent, D. Sage, and M. Unser.** 2004. Complex wavelets for extended depth-of-field: a new method for the fusion of multichannel microscopy images. Microsc. Res. Tech. **65:**33–42.
22. **Gjermansen, M., P. Ragas, C. Sternberg, S. Molin, and T. Tolker-Nielsen.** 2005. Characterization of starvation-induced dispersion in *Pseudomonas putida* biofilms. Environ. Microbiol. **7:**894–906.
23. **Gjermansen, M., P. Ragas, and T. Tolker-Nielsen.** 2006. Proteins with GGDEF and EAL domains regulate *Pseudomonas putida* biofilm formation and dispersal. FEMS Microbiol. Lett. **265:**215–224.
24. Reference deleted.
25. **Harshey, R. M.** 2003. Bacterial motility on a surface: many ways to a common goal. Annu. Rev. Microbiol. **57:**249–273.
26. **Harshey, R. M.** 1994. Bees aren't the only ones: swarming in gram-negative bacteria. Mol. Microbiol. **13:**389–394.
27. **Hartmans, S., M. J. van der Werf, and J. A. de Bont.** 1990. Bacterial degradation of styrene involving a novel flavin adenine dinucleotide-dependent styrene monooxygenase. Appl. Environ. Microbiol. **56:**1347–1351.
28. **Hickman, J. W., D. F. Tifrea, and C. S. Harwood.** 2005. A chemosensory system that regulates biofilm formation through modulation of cyclic diguanylate levels. Proc. Natl. Acad. Sci. USA **102:**14422–14427.
29. **Hoh, J. H., and C. A. Schoenenberger.** 1994. Surface morphology and mechanical properties of MDCK monolayers by atomic force microscopy. J. Cell Sci. **107:**1105–1114.
30. **Ivnitsky, H., I. Katz, D. Minz, G. Volvovic, E. Shimoni, E. Kesselman, R. Semiat, and C. G. Dosoretz.** 2007. Bacterial community composition and structure of biofilms developing on nanofiltration membranes applied to wastewater treatment. Water Res. **41:**3924–3935.
31. **Kang, S. T., A. Subramani, E. M. V. Hoek, M. A. Deshusses, and M. R. Matsumoto.** 2004. Direct observation of biofouling in cross-flow microfiltration: mechanisms of deposition and release. J. Membr. Sci. **244:**151–165.
32. **Klausen, M., M. Gjermansen, J. U. Kreft, and T. Tolker-Nielsen.** 2006. Dynamics of development and dispersal in sessile microbial communities: examples from *Pseudomonas aeruginosa* and *Pseudomonas putida* model biofilms. FEMS Microbiol. Lett. **261:**1–11.
33. **Korber, D. R., J. R. Lawrence, and D. E. Caldwell.** 1994. Effect of motility on surface colonization and reproductive success of *Pseudomonas fluorescens* in dual-dilution continuous-culture and batch culture systems. Appl. Environ. Microbiol. **60:**1421–1429.
34. **Li, H., A. G. Fane, H. G. L. Coster, and S. Vigneswaran.** 1998. Direct observation of particle deposition on the membrane surface during crossflow microfiltration. J. Membr. Sci. **149:**83–97.
35. **Madwar, K., and H. Tarazi.** 2003. Desalination techniques for industrial wastewater reuse. Desalination **152:**325–332.
36. **Matilla, M. A., J. L. Ramos, E. Duque, J. de Dios Alché, M. Espinosa-Urgel, and M. I. Ramos-González.** 2007. Temperature and pyoverdine-mediated iron acquisition control surface motility of *Pseudomonas putida*. Environ. Microbiol. **9:**1842–1850.
37. **Merod, R. T., J. E. Warren, H. McCaslin, and S. Wuertz.** 2007. Towards automated analysis of biofilm architecture: bias caused by extraneous confocal scanning laser microscopy images. Appl. Environ. Microbiol. **73:**4922–4930.
38. **Mueller, L. N., J. F. de Brouwer, J. S. Almeida, L. J. Stal, and J. B. Xavier.** 2006. Analysis of a marine phototrophic biofilm by confocal laser scanning microscopy using the new image quantification software PHLIP. BMC Ecol. **6:**1–15.
39. **Mueller, R. F.** 1996. Bacterial transport and colonization in low nutrient environments. Water Res. **30:**2681–2690.
40. **Neu, T., G. D. Swerhone, and J. R. Lawrence.** 2001. Assessment of lectin-binding analysis for in situ detection of glycoconjugates in biofilm systems. Microbiology **147:**299–313.
41. **Neu, T. R., and J. R. Lawrence.** 1999. Lectin-binding analysis in biofilm systems. Methods Enzymol. **310:**145–152.
42. **O'Toole, G., H. B. Kaplan, and R. Kolter.** 2000. Biofilm formation as microbial development. Annu. Rev. Microbiol. **54:**49–79.
43. **O'Toole, G. A., and R. Kolter.** 1998. Flagellar and twitching motility are necessary for *Pseudomonas aeruginosa* biofilm development. Mol. Microbiol. **30:**295–304.
44. **Otsu, N.** 1979. Threshold selection method from gray-level histograms. IEEE Trans. Syst. Man Cybern. **9:**62–66.
45. **Pang, C. M., P. Y. Hong, H. L. Guo, and W. T. Liu.** 2005. Biofilm formation characteristics of bacterial isolates retrieved from a reverse osmosis membrane. Environ. Sci. Technol. **39:**7541–7550.
46. **Pereira, M. O., M. Kuehn, S. Wuertz, T. Neu, and L. F. Melo.** 2002. Effect of flow regime on the architecture of a *Pseudomonas fluorescens* biofilm. Biotechnol. Bioeng. **78:**164–171.
47. **Pratt, L. A., and R. Kolter.** 1998. Genetic analysis of *Escherichia coli* biofilm formation: roles of flagella, motility, chemotaxis and type I pili. Mol. Microbiol. **30:**285–293.
48. **Purevdorj, B., J. W. Costerton, and P. Stoodley.** 2002. Influence of hydrodynamics and cell signaling on the structure and behavior of *Pseudomonas aeruginosa* biofilms. Appl. Environ. Microbiol. **68:**4457–4464.
49. **Simm, R., J. D. Fetherston, A. Kader, U. Romling, and R. D. Perry.** 2005. Phenotypic convergence mediated by GGDEF-domain-containing proteins. J. Bacteriol. **187:**6816–6823.
50. **Solomon, E. B., and K. R. Matthews.** 2006. Interaction of live and dead *Escherichia coli* O157:H7 and fluorescent microspheres with lettuce tissue suggests bacterial processes do not mediate adherence. Lett. Appl. Microbiol. **42:**88–93.
51. **Song, L. F., and M. Elimelech.** 1995. Particle deposition onto a permeable surface in laminar-flow. J. Colloid Interface Sci. **173:**165–180.
52. **Stoodley, P., K. Sauer, D. G. Davies, and J. W. Costerton.** 2002. Biofilms as complex differentiated communities. Annu. Rev. Microbiol. **56:**187–209.
53. **Tischler, A. D., and A. Camilli.** 2004. Cyclic diguanylate (c-di-GMP) regulates *Vibrio cholerae* biofilm formation. Mol. Microbiol. **53:**857–869.
54. **Tolker-Nielsen, T., U. C. Brinch, P. C. Ragas, J. B. Andersen, C. S. Jacobsen, and S. Molin.** 2000. Development and dynamics of *Pseudomonas* sp. biofilms. J. Bacteriol. **182:**6482–6489.
55. **Turnbull, G. A., J. A. Morgan, J. M. Whipps, and J. R. Saunders.** 2001. The role of motility in the in vitro attachment of *Pseudomonas putida* PaW8 to wheat roots. FEMS Microbiol. Ecol. **35:**57–65.
56. **Watnick, P. I., and R. Kolter.** 1999. Steps in the development of a *Vibrio cholerae* El Tor biofilm. Mol. Microbiol. **34:**586–595.
57. **Wimpenny, J.** 2000. Structural determinants in biofilm formation, p. 466. *In* L. V. Evans (ed.), Biofilms: recent advances in their study and control. Harwood Academic Publishers, Amsterdam, The Netherlands.
58. **Yang, C. H., J. A. Menge, and D. A. Cooksey.** 1994. Mutations affecting hyphal colonization and pyoverdine production in pseudomonads antagonistic toward *Phytophthora parasitica*. Appl. Environ. Microbiol. **60:**473–481.